

The objective deformation component of a velocity field

Bálint Kaszás^{a,*}, Tiemo Pedergnana^b, George Haller^a

^a Institute for Mechanical Systems, ETH Zurich, Zurich, Switzerland

^b Institute for Energy and Process Engineering, ETH Zurich, Zurich, Switzerland



ARTICLE INFO

Article history:

Received 6 May 2022

Received in revised form 29 November 2022

Accepted 12 December 2022

Available online 20 December 2022

Dataset link: [Numerical implementation of the proposed method \(Original data\)](#)

Keywords:

Deformation velocity

Frame indifference

Visualization

ABSTRACT

For an arbitrary velocity field \mathbf{v} defined on a finite, fixed spatial domain, we find the closest rigid-body velocity field \mathbf{v}_{RB} to \mathbf{v} in the L^2 norm. The resulting deformation velocity component, $\mathbf{v}_d = \mathbf{v} - \mathbf{v}_{RB}$, turns out to be frame-indifferent and physically observable. Specifically, if $\mathbf{Q}_{RB}(t)$ is the rotation tensor describing the motion of the closest rigid body frame, then \mathbf{v} is seen as $\mathbf{Q}_{RB}^T \mathbf{v}_d$ by an observer in that frame. As a consequence, the momentum, energy, vorticity, enstrophy, and helicity of the flow all become frame-indifferent when computed from the deformation velocity component \mathbf{v}_d .

© 2022 The Author(s). Published by Elsevier Masson SAS. This is an open access article under the CC BY license (<http://creativecommons.org/licenses/by/4.0/>).

1. Introduction

The analysis of fluid flows often starts with the inspection of the instantaneous spatial features of the velocity field, such as the streamlines, streamsurfaces, as well as the distribution of vorticity, rate of strain, enstrophy and various other scalars used in classic vortex criteria [1–3]. Virtually all these spatial features, however, depend on the observer, and hence do not reflect purely intrinsic properties of the fluid. The independence of material response on the observer, which is usually referred to as frame-indifference or objectivity, is a fundamental axiom of continuum mechanics [4].

Based on physical considerations, one may nevertheless argue for a distinguished frame of reference in which to evaluate customary flow diagnostics. If such a frame exists for the fluid, it is often called the co-moving or proper frame [5].

Finding proper frames is straightforward when there is a homogeneous (periodic or infinite) direction of flow propagation. This is the case for traveling waves or relative periodic orbits in shear flows [6] for which a well-defined base velocity field exists. In some cases, even time-dependent phase speeds c can be found for fluids in a channel, minimizing the difference between the velocity field at x and at $x - ct$, as in [7,8].

For general fluid flows, finding a single co-moving frame in which the fluid velocity field $\mathbf{v}(\mathbf{x}, t)$ becomes simple (or even steady) is unrealistic, as pointed out by Lugt [9]. One may nevertheless seek a rigid-body frame that is overall as close as possible

to being a co-moving frame for the whole fluid. Subtracting such a rigid-body velocity field $\mathbf{v}_{RB}(\mathbf{x}, t)$ from $\mathbf{v}(\mathbf{x}, t)$ would then yield a deformation velocity field that describes the overall deviation of the fluid from rigid body motion as closely as possible. In order for such a decomposition to be meaningful, we propose the following requirements:

- (i) \mathbf{v}_{RB} should be a rigid body velocity field that is closest to \mathbf{v} in a physically relevant norm.
- (ii) $\mathbf{v} - \mathbf{v}_{RB}$ should be frame-indifferent (objective) in order to capture intrinsic features of the fluid (see [10]),
- (iii) $\mathbf{v} - \mathbf{v}_{RB}$ should be physically observable: an appropriately chosen, single observer of the fluid flow should be able to measure this deformation velocity field over the whole domain. Specifically, $\mathbf{v} - \mathbf{v}_{RB}$ should be related to the original velocity field \mathbf{v} under a proper change of observers, i.e. a time dependent Euclidean transformation of the spatial domain.

Available decompositions for velocity fields fail to satisfy these three requirements. An example is the classic Reynolds decomposition (see, e.g., [11]), in which velocity field of a turbulent fluid is written as a sum of its time average and a fluctuating part. As shown in [12], the fluctuating part of the velocity is objective but not physically observable, that is, the total velocity and the fluctuating part are not related to each other via a time dependent Euclidean transformation. The existence of a well-defined time-average is not guaranteed either. Another example, the Helmholtz–Hodge [13] decomposition, splits $\mathbf{v}(\mathbf{x}, t)$ into an incompressible and an irrotational component in a given frame. As a generalization, the Weber–Clebsch representation [14,15]

* Corresponding author.

E-mail address: bkaszas@ethz.ch (B. Kaszás).

has a linear combination of non-potential components. This, however, returns the same flow when the flow is incompressible without extracting any of its deformational features.

The separation of rotations and internal motions is also an important step in the analysis of the n -body problem, as discussed, for example, in [16]. There, an appropriate choice of the reference frame makes it possible to write the Lagrangian as a sum of rotational and deformational components. Further local decompositions seek to isolate rotational velocity components based on the velocity gradient. Examples include the deformation-rotation decomposition of Batchelor [17] and the procedures of Kolář [18], Liu et al. [19], Wang et al. [20] and Holmedal [21]. In the Lagrangian frame, only infinitesimal decompositions of the flow have been obtained. The closest of these in spirit to the present study is the polar decomposition, which yields a polar rotation tensor that is pointwise the closest rigid-body rotation to the deformation gradient [22].

In a recent stream of papers in the scientific visualization community, Bujack et al. [23], Günther et al. [24], Kim and Günther [25], Rojo and Günther [26] and Günther and Theisel [27] seek an objectively defined minimally unsteady component $\mathbf{v}_*(\mathbf{x}, t)$ of $\mathbf{v}(\mathbf{x}, t)$. Haller [28] shows that the proposed implementations of these principles leads to $\mathbf{v}_*(\mathbf{x}, t) \equiv \mathbf{v}(\mathbf{x}, t)$ and hence fail to provide the desired decomposition. Using a simple counterexample, Haller [28] also shows that even under a correct implementation, $\mathbf{v}_*(\mathbf{x}, t)$ would not be objective, irrespective of the measure of unsteadiness chosen. Theisel et al. [29] continue to claim objectivity of $\mathbf{v}_*(\mathbf{x}, t)$, but their argument uses the pull-back, as opposed to the inverse, of the nonlinear transformation $\mathbf{v} \mapsto \mathbf{v}_*$ when computing $\mathbf{v}_* \mapsto \mathbf{v}$. This is incorrect, given that velocity fields are non-objective precisely because they do not transform under the push-forward and pull-back of frame changes.

In a parallel development, Hadwiger et al. [30], Rautek et al. [31], and Zhang et al. [32] seek a nonlinear (i.e., non-rigid-body) observer velocity field $\mathbf{u}(\mathbf{x}, t)$ that is simultaneously close to \mathbf{v} , has small rate of strain and yields a small Lie-derivative for $\mathbf{v}-\mathbf{u}$ along \mathbf{u} . While these individual objectives all come with their own user-dependent weight functions, the relative velocity $\mathbf{v}-\mathbf{u}$ can indeed be shown to be objective, as long as the optimization principle has a globally unique solution (as assumed but not verified by the authors). The frame change represented by \mathbf{u} , however, is nonlinear and hence $\mathbf{v}-\mathbf{u}$ cannot be observed by any single physical observer. Thus, requirement (iii) is not satisfied.

An alternative idea is to perform pointwise local velocity field decompositions in the flow by passing to local frames co-rotating with the eigenvectors of the rate-of-strain tensor [33–35]. While these pointwise frame changes are individually objective, they are not observable by a single physical observable and cannot be stitched up to form a smoothly varying global coordinate change [28]. In contrast, the vortex criteria developed in [36–39] can be viewed as evaluations of classic vortex criteria in a frame generated by the spin-deviation tensor, as shown by Haller [28]. This frame, however, is not obtained as a closest rigid body frame from any systematic optimization and hence fails to satisfy the requirement (i) above.

In this paper, we derive a closed form solution for a rigid-body velocity component $\mathbf{v}_{RB}(\mathbf{x}, t)$ satisfying the requirements (i)–(iii) on a bounded spatial domain $U \subset \mathbb{R}^3$. We achieve this by explicitly solving the underlying optimization problem defining $\mathbf{v}_{RB}(\mathbf{x}, t)$. We then show that $\mathbf{v}_d = \mathbf{v} - \mathbf{v}_{RB}$ is observer-indifferent and directly observable in a specific Euclidean observer frame. The rigid body velocity \mathbf{v}_{RB} is closest to \mathbf{v} in the classic L^2 norm.

All classic non-objective vortex criteria become objective when evaluated in the frame co-moving with $\mathbf{v}_{RB}(\mathbf{x}, t)$. However, it is still not guaranteed that the objectivized vortex-criteria correctly identify all eddies. Specifically, while after objectivization all

observers will agree on the conclusions of the vortex criteria, the classic criteria we have reviewed still lack a rigorous connection to material behavior in the fluid.

In addition, passage to the deformation velocity preserves the rate-of-strain tensor of the full velocity field, causing \mathbf{v}_d and \mathbf{v} to have the same objective Eulerian coherent structures (OECSs), as defined by Serra and Haller [40]. Similarly, the instantaneous vorticity deviation (IVD) defined by Haller et al. [3], another objective indicator of Eulerian coherence, is also preserved from \mathbf{v} for \mathbf{v}_d by our decomposition.

Perhaps most importantly, all common non-objective Eulerian scalar quantities, such as the kinetic energy, enstrophy, and helicity, become observer-independent when they are evaluated on the deformation velocity $\mathbf{v}_d(\mathbf{x}, t)$. This gives a natural way to define the deformation kinetic energy, deformation enstrophy and deformation helicity of the flow as intrinsic physical quantities that do not depend on the observer.

The optimization with respect to the physically motivated L^2 norm yields a rigid-body velocity field, \mathbf{v}_{RB} , that is uniquely determined over a given spatial domain U . For most problems, the velocity field is a priori given over a certain domain of interest, which defines U as well. Therefore the deformation velocity $\mathbf{v}_d = \mathbf{v} - \mathbf{v}_{RB}$ can be uniquely associated to the velocity field \mathbf{v} .

However, when one has some freedom in choosing the spatial domain U , we show that this choice can influence the deformation velocity \mathbf{v}_d . Specifically, if one chooses a large enough domain for a complicated flow, it is unlikely that passing to a single distinguished reference frame could eliminate all rotating motions simultaneously. Through an example, we show that in oceanographic applications this is indeed the case. Due to the multitude of mesoscale eddies, there is no optimal way to isolate a single rigid-body observer and we obtain $\mathbf{v}_{RB} \approx 0$. If, however, smaller domains with well defined rotational features are of interest in a given problem, then the method successfully extracts a non-zero rigid-body velocity. Choosing the spatial domain U optimally remains a challenge for general flows.

2. Main results

We seek the rigid body velocity field $\mathbf{v}_{RB}(\mathbf{x}, t)$ closest to an arbitrary mass-preserving velocity field $\mathbf{v}(\mathbf{x}, t)$ defined on a bounded (and potentially time-dependent) spatial domain $U \subset \mathbb{R}^3$. To measure closeness between two velocity fields, we use the L^2 norm

$$\|\mathbf{f}\|_{L^2}^2 := \frac{1}{M} \int_U |\mathbf{f}(\mathbf{x}, t)|^2 dm, \tag{1}$$

where M is the total mass contained in the domain U . We use a mass-based, as opposed to the customary volume-based, norm to cover compressible but mass-preserving flows. For incompressible flows, our mass-based minimization is equivalent to a volume-based minimization.

As any rigid body velocity field, the \mathbf{v}_{RB} we seek must have the general form

$$\mathbf{v}_{RB}(\mathbf{x}, t) = \dot{\mathbf{x}}_A(t) + \Omega(t) (\mathbf{x} - \mathbf{x}_A(t)) = \dot{\mathbf{x}}_A(t) + \omega(t) \times (\mathbf{x} - \mathbf{x}_A(t)), \tag{2}$$

where $\mathbf{x}_A(t) \in U$ is the current position of a material point on the rigid body whose instantaneous velocity is $\dot{\mathbf{x}}_A(t)$; $\mathbf{x} \in U$ is another, arbitrary material point on the rigid body, whose instantaneous velocity is $\mathbf{v}_{RB}(\mathbf{x}, t)$. The vector $\omega(t) \in \mathbb{R}^3$ denotes the angular velocity of the rigid body and the skew-symmetric tensor $\Omega(t) = -\Omega^T(t) \in \mathbb{R}^{3 \times 3}$ is defined as

$$\Omega(t)\mathbf{e} = \omega(t) \times \mathbf{e}, \quad \forall \mathbf{e} \in \mathbb{R}^3. \tag{3}$$

More generally, a vector $\omega(t)$ defined by the relation (3) is called the *dual vector* of a skew-symmetric matrix $\Omega(t)$ (see, e.g., [13]). We will use $\omega(t)$ and $\Omega(t)$ interchangeably: all results formulated in terms of the tensor $\Omega(t)$ can be recast in terms of $\omega(t)$ using the formula (3) and vice versa.

We will show that the tuple $(\Omega(t), \mathbf{x}_A(t))$, for which the distance

$$L(\Omega, \mathbf{x}_A, t) = \|\mathbf{v}(\mathbf{x}, t) - \mathbf{v}_{RB}(\mathbf{x}, t)\|_{L^2}^2 \tag{4}$$

is minimal, can be computed explicitly in terms of only the velocity field $\mathbf{v}(\mathbf{x}, t)$ and its domain of definition U . To motivate the choice of the L^2 norm in (4), we note that (4) is proportional to the kinetic energy of $\mathbf{v} - \mathbf{v}_{RB}$. This means that we seek the rigid-body velocity \mathbf{v}_{RB} that minimizes the kinetic energy of the velocity field seen from that rigid body. More general (albeit less physical) norms could also be considered, but they do not change the results significantly, as we show in Appendix G.

The final result from the minimization of $L(\Omega, \mathbf{x}_A, t)$ will depend on the moment of inertia tensor

$$\Theta := \overline{M(|\mathbf{x} - \bar{\mathbf{x}}|^2) \mathbf{I} - (\mathbf{x} - \bar{\mathbf{x}}) \otimes (\mathbf{x} - \bar{\mathbf{x}})}, \tag{5}$$

where overbar denotes mass-based averaging over U (as in (1)), $\mathbf{I} \in \mathbb{R}^{3 \times 3}$ denotes the identity tensor. This is exactly the classic moment of inertia tensor of a rigid body, computed formally with respect to the center of mass $\bar{\mathbf{x}}$ of the fluid mass filling U .

We show in Section 3 that, the closed form solution for the minimizer of (4) is

$$\begin{aligned} \mathbf{x}_A(t) &= \bar{\mathbf{x}}(t), \\ \omega(t) &= M \Theta^{-1}(\overline{(\mathbf{x} - \bar{\mathbf{x}}) \times (\mathbf{v} - \bar{\mathbf{v}})}). \end{aligned} \tag{6}$$

As we will point out in Section 3, the tuple in Eq. (6) optimizes the L^2 distance of $\mathbf{v}_{RB}(\mathbf{x}, t)$ from $\mathbf{v}(\mathbf{x}, t)$ on average over any finite time interval $[t_0, t_1]$, not just at a discrete time $t \in [t_0, t_1]$.

By Eq. (6), the reference point $\mathbf{x}_A(t)$ can be chosen as the center of mass of the fluid, and the optimal rigid-body angular velocity, $\omega(t)$, is a linear function of the velocity field $\mathbf{v}(\mathbf{x}, t)$. Note that the vector $\mathbf{L} = M(\overline{(\mathbf{x} - \bar{\mathbf{x}}) \times (\mathbf{v} - \bar{\mathbf{v}})})$ is the angular momentum of the fluid with respect to its center of mass [41]. Therefore, the angular velocity $\omega(t)$ of the closest rigid body motion obeys the equation $\Theta \omega = \mathbf{L}$, as expected from classical rigid-body mechanics. We emphasize, however, that we have arrived at this result by interpreting the exact solution of the underlying variational principle rather than by analogy.

We now define the deformation component of the velocity (or *deformation velocity*), \mathbf{v}_d , as the difference of \mathbf{v} from \mathbf{v}_{RB} :

$$\mathbf{v}_d(\mathbf{x}, t) := \mathbf{v}(\mathbf{x}, t) - \mathbf{v}_{RB}(\mathbf{x}, t) = \mathbf{v}(\mathbf{x}, t) - \bar{\mathbf{v}}(t) - \omega(t) \times (\mathbf{x} - \bar{\mathbf{x}}(t)). \tag{7}$$

By construction, \mathbf{v}_{RB} satisfies the requirement (i) we have laid down for a meaningful decomposition of \mathbf{v} in Section 1. In Section 3 we will show that additional requirements (ii) and (iii) also hold. Specifically, while the angular velocity $\omega(t)$ is not objective, $\mathbf{v}_d(\mathbf{x}, t)$ is nevertheless an objective vector field and can be observed physically in a frame co-rotating with $\mathbf{v}_{RB}(\mathbf{x}, t)$.

Discrete versions of Eq. (6) defining the angular velocity vector also appear in the n -body problem (see, e.g., Tachibana and Iwai [42] and Marsden [43]), where separating rotational and deformational degrees of freedom is essential. In that setting, passing to a (possibly time-dependent) body frame decomposes the kinetic energy into two terms: one comes from rotations, and the other comes from changes in the shape of the n -body system (i.e., deformations). Eckart [44] gives a standard method of choosing the body frame. Moreover, this separation of the kinetic energy (and hence the n -body Lagrangian) is shown by Littlejohn and Reinsch [16] to be gauge invariant. Since the gauge convention refers to choosing the body frame, gauge invariance is

the same as objectivity in the language of continuum mechanics. Our results, however, are indifferent to the underlying Lagrangian of the system. The decomposition defined by Eq. (7) can be applied to arbitrary velocity fields, even to those obtained from measurements.

Velocity fields with similar names have appeared in other contexts before, such as Bergeron [45]’s deformation field for frontogenesis (see also [4,46]). However, in that case, *deformation field* refers to a specific velocity field that induces deformation. Our Eq. (7) instead defines a deformation velocity associated to any given velocity field \mathbf{v} .

The results outlined above enable us to *objectivize* a number of originally non-objective scalar-, vector- and tensor-fields derived from $\mathbf{v}(\mathbf{x}, t)$ by computing these fields in the frame co-moving with \mathbf{v}_{RB} . In practice, this simply means computing the fields from $\mathbf{v}_d(\mathbf{x}, t)$ as opposed to $\mathbf{v}(\mathbf{x}, t)$. Examples of scalar fields that become objective in this fashion include the kinetic energy, enstrophy, and helicity. Similarly, when computed in the frame co-moving with \mathbf{v}_{RB} , the vorticity, linear momentum and angular momentum become objective vector fields and the velocity gradient and the spin tensor become objective tensor fields. For instance, the *deformation kinetic energy*

$$E_d(t) = \frac{1}{2} \int_U |\mathbf{v}_d(\mathbf{x}, t)|^2 \tag{8}$$

is a frame-invariant measure of the kinetic energy related to flow deformation. One may, for instance, plot this scalar field to reveal observer-independent Eulerian features of the flow that arise from fluid deformation rather than rigid-body translation and rotation.

3. Derivation of the main results

We now present the derivation of our main results discussed in Section 2.

3.1. Solution to the optimization problem

After substitution of the general expression of the rigid body velocity field (2) into the distance functional $L(\Omega, \mathbf{x}_A, t)$ defined in Eq. (4), we obtain

$$\begin{aligned} L_1(\Omega, t) &= \|\mathbf{v}(\mathbf{x}, t) - \mathbf{v}_{RB}(\mathbf{x}, t)\|_{L^2}^2 \\ &= \frac{1}{M} \int_U \{|\mathbf{v}(\mathbf{x}, t) - \dot{\mathbf{x}}_A(t) - \Omega(t)(\mathbf{x} - \mathbf{x}_A(t))|^2\} \rho(\mathbf{x}, t) dV \end{aligned} \tag{9}$$

where $\rho(\mathbf{x}, t)$ is the density of the (potentially compressible) fluid.

As we will see, the solution of the minimization problem $L_1(\Omega, t)$ will yield a unique closest rigid body motion, but any point of that body can be chosen as the reference point $\mathbf{x}_A(t)$. Indeed, if a given pairing $(\mathbf{x}_A(t), \Omega(t))$ generates the closest rigid-body motion to $\mathbf{v}(\mathbf{x}, t)$, then all pairs $(\mathbf{x}_B(t), \Omega(t))$ will qualify as well, as long as

$$\dot{\mathbf{x}}_B(t) = \dot{\mathbf{x}}_A(t) + \Omega(t)(\mathbf{x}_B(t) - \mathbf{x}_A(t))$$

holds, i.e., $(\mathbf{x}_B(t), \Omega(t))$ describe the same rigid body motion. The most straightforward choice for $\mathbf{x}_A(t)$ is the center of mass of the fluid, i.e.,

$$\mathbf{x}_A(t) = \bar{\mathbf{x}}(t) = \frac{1}{M} \int_U \mathbf{x} dm = \frac{1}{M} \int_U \mathbf{x} \rho(\mathbf{x}, t) dV.$$

As the total mass of the fluid is assumed to be constant, we then have

$$\dot{\mathbf{x}}_A(t) = \frac{D}{Dt} \bar{\mathbf{x}}(t) = \frac{D}{Dt} \frac{1}{M} \int_U \mathbf{x} dm = \frac{1}{M} \int_U \frac{D}{Dt} \mathbf{x} dm$$

$$\begin{aligned}
 &= \frac{1}{M} \int_U \mathbf{v}(\mathbf{x}, t) \, dm = \frac{1}{M} \int_U \mathbf{v}(\mathbf{x}, t) \rho(\mathbf{x}, t) \, dV \\
 &= \bar{\mathbf{v}}(t),
 \end{aligned}$$

where $\bar{\mathbf{v}}(t)$ denotes the mass-based (or density-weighted) average of the velocity field over U . For incompressible flows, this $\bar{\mathbf{v}}$ also agrees with the spatial average of \mathbf{v} over the domain U .

Therefore, the closest rigid-body motion to $\mathbf{v}(\mathbf{x}, t)$, without loss of generality, can be sought in the more specific form

$$\mathbf{v}_{RB}(\mathbf{x}, t) = \bar{\mathbf{v}}(t) + \boldsymbol{\Omega}(t) (\mathbf{x} - \bar{\mathbf{x}}(t)), \tag{10}$$

where $\boldsymbol{\Omega}(t)$ is the global minimizer of the functional $L_1(\boldsymbol{\Omega}, t)$ defined in Eq. (9). Such a unique global minimizer must solve the associated Euler–Lagrange equation

$$\frac{\partial}{\partial \boldsymbol{\Omega}} L_1(\boldsymbol{\Omega}, t) = 0. \tag{11}$$

This last equation is also the Euler–Lagrange equation associated with the problem of extremizing the functional $\frac{1}{t_1-t_0} \int_{t_0}^{t_1} L_1(\boldsymbol{\Omega}(t), t) dt$. Therefore, Eq. (11) provides a solution $\boldsymbol{\Omega}(t)$ that optimizes the L^2 distance of $\mathbf{v}_{RB}(\mathbf{x}, t)$ from $\mathbf{v}(\mathbf{x}, t)$ on average over any finite time interval $[t_0, t_1]$, not just at a discrete time $t \in [t_0, t_1]$.

To calculate the minimizing $\boldsymbol{\Omega}(t)$ explicitly, we express $L_1(\boldsymbol{\Omega}, t)$ in coordinates. We will only focus on the additive terms of $L_1(\boldsymbol{\Omega}, t)$ that depend on $\boldsymbol{\Omega}$, collecting them in a functional $\tilde{L}_1(\boldsymbol{\Omega}, t)$ with $\frac{\partial}{\partial \boldsymbol{\Omega}} [L_1 - \tilde{L}_1] \equiv \mathbf{0}$. This \tilde{L}_1 can be written as

$$\begin{aligned}
 \tilde{L}_1(\boldsymbol{\Omega}, t) = \frac{1}{M} \int_U \{ &-2(v_i - \dot{x}_i) \Omega_{ij} (x_j - \bar{x}_j) \\
 &+ \Omega_{ij} (x_j - \bar{x}_j) \Omega_{ik} (x_k - \bar{x}_k) \} \rho \, dV, \tag{12}
 \end{aligned}$$

with summation implied over repeated indices. As we show in Appendix A, substitution of Eq. (12) into (11) leads to a lengthy expression which can nevertheless be simplified in invariant form to

$$\overline{(\mathbf{x} - \bar{\mathbf{x}}) \times (\mathbf{v} - \bar{\mathbf{v}})} = \overline{(|\mathbf{x} - \bar{\mathbf{x}}|^2) \boldsymbol{\omega} - (\mathbf{x} - \bar{\mathbf{x}}) \otimes (\mathbf{x} - \bar{\mathbf{x}}) \boldsymbol{\omega}} \tag{13}$$

where the angular velocity $\boldsymbol{\omega}(t)$ is an extremizer of \tilde{L}_1 . We can write the right-hand side of Eq. (13) as $\frac{1}{M} \boldsymbol{\Theta} \boldsymbol{\omega}$ using the moment of inertia tensor defined in (5). As the classic moment of inertia tensor, $\boldsymbol{\Theta}$, is positive definite by construction, it is also invertible for all times t . Then, multiplication of both sides of (13) by $M \boldsymbol{\Theta}^{-1}$ gives the closest rigid-body angular velocity

$$\boldsymbol{\omega} = M \boldsymbol{\Theta}^{-1} \overline{(\mathbf{x} - \bar{\mathbf{x}}) \times (\mathbf{v} - \bar{\mathbf{v}})}, \tag{14}$$

a linear function of the velocity field \mathbf{v} .

In order to check whether the angular velocity vector defined by (14) is a minimizer of the functional \tilde{L}_1 , it is sufficient to note that its Hessian is

$$\frac{\partial^2}{\partial \omega_n \partial \omega_p} \tilde{L}_1(\boldsymbol{\omega}, t) = \frac{2}{M} [\boldsymbol{\Theta}]_{np},$$

with the details of this calculation given in Appendix B. By the positive definiteness of $\boldsymbol{\Theta}$ we conclude that $\tilde{L}_1(\boldsymbol{\omega}, t)$ indeed has a unique, strict global minimum at the rigid-body angular velocity $\boldsymbol{\omega}$ defined in (14).

3.2. Properties of the deformation velocity

3.2.1. Basic properties of \mathbf{v}_d

We note that the deformation velocity is guaranteed to have no further rigid-body velocity component under our decomposition principle. Indeed, applying formulas (14) and (7) again to $\mathbf{v} = \mathbf{v}_d$ would yield the secondary rigid-body angular velocity

$$\boldsymbol{\omega}^{(2)} = \mathbf{0},$$

as we show in detail in Appendix F.

3.2.2. Objectivity of \mathbf{v}_d

We recall that a vector field $\mathbf{a}(\mathbf{x}, t)$ is said to be *objective* if under any Euclidean transformation

$$\mathbf{x} = \mathbf{Q}(t) \mathbf{y} + \mathbf{b}(t), \quad \mathbf{Q} \mathbf{Q}^T = \mathbf{I}, \quad \mathbf{Q}(t) \in \text{SO}(3), \quad \mathbf{y}, \mathbf{b}(t) \in \mathbb{R}^3, \tag{15}$$

it transforms as

$$\hat{\mathbf{a}}(\mathbf{y}, t) = \mathbf{Q}^T(t) \mathbf{a}(\mathbf{x}, t), \tag{16}$$

In the transformed frame defined by (15) the transformed rigid-body angular velocity, $\boldsymbol{\omega}$, satisfies

$$\widehat{\boldsymbol{\Theta}} \hat{\boldsymbol{\omega}} = M \overline{(\mathbf{y} - \bar{\mathbf{y}}) \times (\hat{\mathbf{v}} - \hat{\bar{\mathbf{v}}})}, \tag{17}$$

with

$$\widehat{\boldsymbol{\Theta}} = M \overline{(|\mathbf{y} - \bar{\mathbf{y}}|^2) \mathbf{I} - (\mathbf{y} - \bar{\mathbf{y}}) \otimes (\mathbf{y} - \bar{\mathbf{y}})}. \tag{18}$$

The moment of inertia tensor $\boldsymbol{\Theta}$ is an objective tensor [16], i.e., transforms as

$$\widehat{\boldsymbol{\Theta}} = \mathbf{Q}^T \boldsymbol{\Theta} \mathbf{Q}. \tag{19}$$

Differentiation of Eq. (15) with respect to time gives the classic velocity transformation rule,

$$\hat{\mathbf{v}} = \mathbf{Q}^T (\mathbf{v} - \dot{\mathbf{Q}} \mathbf{y} - \dot{\mathbf{b}}), \tag{20}$$

which enables us to conclude in Appendix C that the closest rigid-body angular velocity transforms as

$$\hat{\boldsymbol{\omega}} = \mathbf{Q}^T (\boldsymbol{\omega} - \dot{\mathbf{q}}), \tag{21}$$

where $\dot{\mathbf{q}}(t)$ is the dual of the skew-symmetric matrix $\dot{\mathbf{Q}} \mathbf{Q}^T(t)$.

In the \mathbf{y} -frame, the deformation velocity defined by Eq. (7) is simply

$$\hat{\mathbf{v}}_d = \hat{\mathbf{v}} - \hat{\bar{\mathbf{v}}} - \hat{\boldsymbol{\omega}} \times (\mathbf{y} - \bar{\mathbf{y}}). \tag{22}$$

Substituting the transformation rules (20) and (21) for \mathbf{v} , $\boldsymbol{\omega}$ and $\bar{\mathbf{v}}$ into Eq. (22), we then obtain in Appendix D that

$$\hat{\mathbf{v}}_d = \mathbf{Q}^T \mathbf{v}_d. \tag{23}$$

Therefore, by formula (16), the deformation velocity \mathbf{v}_d is objective.

3.2.3. Physical observability of \mathbf{v}_d

We now consider the specific frame change

$$\mathbf{x} = \mathbf{Q}_{RB}(t) \mathbf{y} + \mathbf{b}_{RB}(t), \tag{24}$$

with $\mathbf{Q}_{RB}(t)$ and $\mathbf{b}_{RB}(t)$ defined as solutions of the linear system of differential equations

$$\begin{aligned}
 \dot{\mathbf{Q}}_{RB} &= \boldsymbol{\Omega}(t) \mathbf{Q}_{RB}, \\
 \dot{\mathbf{b}}_{RB} &= \boldsymbol{\Omega}(t) \mathbf{b}_{RB}(t) + \bar{\mathbf{v}}(t) - \boldsymbol{\Omega}(t) \bar{\mathbf{x}},
 \end{aligned} \tag{25}$$

satisfying the initial conditions $\mathbf{Q}_{RB}(t_0) = \mathbf{I}$ and $\mathbf{b}_{RB}(t_0) = \mathbf{0}$. In (25), we used the tensorial form of the rigid body velocity, i.e., $\boldsymbol{\Omega}$ is the dual of $\boldsymbol{\omega}$, as defined by formula (3). Note that $\boldsymbol{\Omega}(t)$ is skew-symmetric and hence the fundamental solution of the first equation in (25) is automatically proper orthogonal. The second equation in (25) is also linear and hence has a unique solution $\mathbf{b}_{RB}(t)$ for the initial conditions specified.

As we show in Appendix E, under the observer change (24), the full velocity field becomes

$$\hat{\mathbf{v}} = \mathbf{Q}_{RB}^T \mathbf{v}_d. \tag{26}$$

At the same time, the general transformation formula (23) evaluated on the specific frame change (24) gives $\hat{\mathbf{v}}_d = \mathbf{Q}_{RB}^T \mathbf{v}_d$, and hence Eq. (26) implies

$$\hat{\mathbf{v}} = \hat{\mathbf{v}}_d = \mathbf{Q}_{RB}^T \mathbf{v}_d. \tag{27}$$

Therefore, the full velocity field coincides with its deformation velocity component in the frame of the specific observer defined by the linear ODEs in (25). This is because the specific frame change (25) eliminates both the mean velocity and the mean vorticity in the \mathbf{y} frame, which makes the velocity field identical to its deformation part. This special frame, therefore, is the frame co-moving with the closest rigid-body velocity field \mathbf{v}_{RB} .

All this also implies that the trajectories of the ODE

$$\dot{\mathbf{y}} = \mathbf{Q}_{RB}^T(t)\mathbf{v}_d(\mathbf{Q}_{RB}(t)\mathbf{y} + \mathbf{b}_{RB}(t), t) \tag{28}$$

are mapped into the trajectories of the original velocity field $\mathbf{v}(\mathbf{x}, t)$ under the change of variables (24). Therefore, the trajectories of (28) are smoothly conjugate to those of $\mathbf{v}(\mathbf{x}, t)$, sharing the same dynamic features as trajectories of conjugate dynamical systems always do (stability, asymptotic behavior, invariant manifolds etc.). As any frame change, the transformation (24) also transforms originally fixed flow boundaries (as invariant manifolds of the flow) into moving invariant surfaces. Note, however, that there is, in general, no smooth conjugacy between the trajectories of \mathbf{v} and those of \mathbf{v}_d .

3.3. Objectivization of physical fields using the deformation velocity

The most broadly used Eulerian quantities (e.g., the kinetic energy, momentum and vorticity) associated with a moving fluid depend on the observer and hence do not capture purely intrinsic properties of the flow. The objectivity of the deformation velocity \mathbf{v}_d , however, makes it possible to eliminate this observer dependence by simply computing these classic Eulerian quantities from \mathbf{v}_d as opposed to \mathbf{v} . In view of formula (27), the replacement of \mathbf{v} with \mathbf{v}_d is equivalent to evaluating the original non-objective quantities in a special, objectively determined frame that is uniquely identifiable by any physical observer.

Specifically, the pointwise deformation kinetic energy, $E_d(\mathbf{x}, t)$, deformation enstrophy, $\mathcal{E}_d(\mathbf{x}, t)$, and deformation helicity, $H_d(\mathbf{x}, t)$, can be defined by evaluating their classic counterparts, $E = \frac{1}{2}|\mathbf{v}|^2$, $\mathcal{E} = |\nabla \times \mathbf{v}|^2$ and $H = |\mathbf{v} \cdot \nabla \times \mathbf{v}|^2$, in the frame co-moving with $\mathbf{v}_{RB}(\mathbf{x}, t)$, as defined in Eq. (24). The scalar fields

$$\begin{aligned} E_d(\mathbf{x}, t) &= \frac{1}{2} |\hat{\mathbf{v}}(\mathbf{y}, t)|^2 = \frac{1}{2} |\mathbf{v}_d(\mathbf{x}, t)|^2, \\ \mathcal{E}_d(\mathbf{x}, t) &= \left| \hat{\nabla} \times \hat{\mathbf{v}}(\mathbf{y}, t) \right|^2 = |\nabla \times \mathbf{v}_d(\mathbf{x}, t)|^2, \\ H_d(\mathbf{x}, t) &= \left| \hat{\mathbf{v}}(\mathbf{y}, t) \cdot \hat{\nabla} \times \hat{\mathbf{v}}(\mathbf{y}, t) \right|^2 = |\mathbf{v}_d(\mathbf{x}, t) \cdot \nabla \times \mathbf{v}_d(\mathbf{x}, t)|^2, \end{aligned} \tag{29}$$

are objective, returning pointwise energy, enstrophy and helicity values that are independent of the observer. This also means that the various topological features (such as the level sets) of these fields are indifferent to changes in the observer and hence are intrinsic to the fluid, unlike those of $E(\mathbf{x}, t)$, $\mathcal{E}(\mathbf{x}, t)$, and $H(\mathbf{x}, t)$. The spatial integrals of the Eulerian scalar fields in (29) over the flow domain U are also frame-invariant, given the pointwise objectivity of their integrands.

As an exception, the turbulent kinetic energy,

$$k(\mathbf{x}, t) = \frac{1}{T} \int_t^{t+T} \left| \mathbf{v}(\mathbf{x}, \tau) - \frac{1}{T} \int_\tau^{\tau+T} \mathbf{v}(\mathbf{x}, s) ds \right|^2 d\tau,$$

whose definition relies on the assumption of a well-defined temporal mean at each point of the flow [11], does not become objective even when evaluated on \mathbf{v}_d . Indeed, in a transformed frame, we would have

$$\hat{k}_d = \frac{1}{T} \int_t^{t+T} \left| \hat{\mathbf{v}}_d(\mathbf{y}, \tau) - \frac{1}{T} \int_\tau^{\tau+T} \hat{\mathbf{v}}_d(\mathbf{y}, s) ds \right|^2 d\tau$$

$$\begin{aligned} &= \frac{1}{T} \int_t^{t+T} \left| \mathbf{Q}^T(\tau)\mathbf{v}_d(\mathbf{y}, \tau) - \frac{1}{T} \int_\tau^{\tau+T} \mathbf{Q}^T(s)\mathbf{v}_d(\mathbf{y}, s) ds \right|^2 d\tau \\ &= \frac{1}{T} \int_t^{t+T} \left| \mathbf{v}_d(\mathbf{y}, \tau) - \frac{1}{T} \mathbf{Q}(\tau) \int_\tau^{\tau+T} \mathbf{Q}^T(s)\mathbf{v}_d(\mathbf{y}, s) ds \right|^2 d\tau \\ &\neq k_d. \end{aligned}$$

In contrast, the deformation momentum \mathbf{p}_d and the deformation vorticity \mathbf{w}_d , defined as

$$\begin{aligned} \mathbf{p}_d(\mathbf{x}, t) &= \rho(\mathbf{x}, t)\mathbf{v}_d(\mathbf{x}, t), \\ \mathbf{w}_d(\mathbf{x}, t) &= \nabla \times \mathbf{v}_d(\mathbf{x}, t), \end{aligned}$$

become objective vector fields. This follows from the objectivity of \mathbf{v}_d established in formula (23). Likewise, the deformation velocity gradient, $\nabla \mathbf{v}_d$, the deformation rate-of-strain tensor $\mathbf{S}_d = \frac{1}{2}(\nabla \mathbf{v}_d + [\nabla \mathbf{v}_d]^T)$ and the deformation spin tensor, $\mathbf{W}_d = \frac{1}{2}(\nabla \mathbf{v}_d - [\nabla \mathbf{v}_d]^T)$ are all objective tensors. In addition, we have

$$\mathbf{S}_d(\mathbf{x}, t) \equiv \mathbf{S}(\mathbf{x}, t), \tag{30}$$

where $\mathbf{S} = \frac{1}{2}(\nabla \mathbf{v} + [\nabla \mathbf{v}]^T)$ is the classic rate-of-strain tensor.

A consequence of Eq. (30) is that the deformation velocity also contains all objective Eulerian coherent structures (OECS; see [40]) of the original velocity field. These coherent structures are defined as the instantaneous limits of Lagrangian coherent structures (LCSs; see [47]) and hence govern the advection of material fluid elements for short times. Passage to the deformation velocity also preserves another Eulerian indicator of coherence, the instantaneous vorticity deviation $\text{IVD}(\mathbf{x}, t) = \frac{1}{2} |\mathbf{w}(\mathbf{x}, t) - \overline{\mathbf{w}}(\mathbf{x}, t)|$, defined by Haller et al. [3]. Indeed,

$$\text{IVD}_d = \frac{1}{2} |\mathbf{w}_d - \overline{\mathbf{w}}_d| = \frac{1}{2} |\mathbf{w} - 2\omega - \overline{\mathbf{w}} + 2\omega| = \text{IVD}.$$

More generally, even though they often lack a rigorous connection to the flow, all the classic vortex criteria reviewed in [18,48,49], and [28] become indifferent to the observer when evaluated on \mathbf{v}_d , or, equivalently, on the full velocity field in a frame co-moving with \mathbf{v}_{RB} .

As a Lagrangian example, we recall the trajectory length function proposed by Mancho et al. [50], defined as

$$M_{t_0}^{t_1}(\mathbf{x}_0) = \int_{t_0}^{t_1} |\mathbf{v}(\mathbf{x}(s; \mathbf{x}_0), s)| ds. \tag{31}$$

Evaluating (32) on \mathbf{v}_d makes $M_{t_0}^{t_1}$ objective. Indeed, as $\hat{\mathbf{v}}_d = \mathbf{Q}^T \mathbf{v}_d$, the transformed trajectory length is

$$\hat{M}_{t_0}^{t_1}(\mathbf{y}_0) = \int_{t_0}^{t_1} |\hat{\mathbf{v}}_d(\mathbf{y}(s; \mathbf{y}_0), s)| ds = M_{t_0}^{t_1}(\mathbf{x}_0). \tag{32}$$

4. Examples

We now briefly illustrate the extraction of deformation velocities in two-dimensional and three-dimensional examples.

4.1. Deformation velocities in 2D

First, we perform the proposed velocity decomposition on two of the explicit two-dimensional unsteady Navier–Stokes solutions derived in [51]. Our first example is the velocity field

$$\begin{aligned} \mathbf{v}(\mathbf{x}, t) &= \begin{pmatrix} \dot{x} \\ \dot{y} \end{pmatrix} = \begin{pmatrix} \sin 4t & \cos 4t + 2 \\ \cos 4t - 2 & -\sin 4t \end{pmatrix} \begin{pmatrix} x \\ y \end{pmatrix} \\ &\quad + 0.005 \begin{pmatrix} x(x^2 - 3y^2) \\ -x(3x^2 - y^2) \end{pmatrix}. \end{aligned} \tag{33}$$

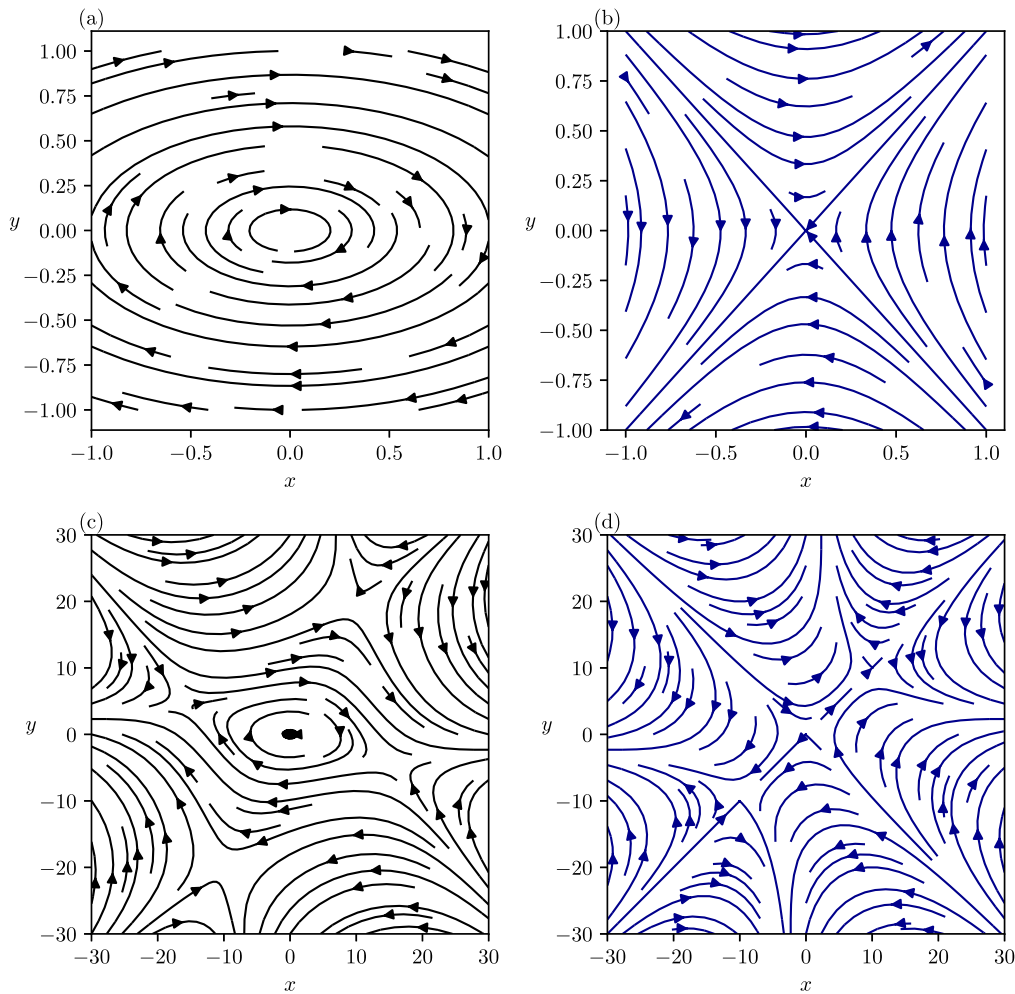


Fig. 1. Left column: Observer-dependent streamlines of the velocity field (33) over the domains U_1 (a) and U_{30} (c). Right column: Objective streamlines of the corresponding deformation velocity field $\mathbf{v}_d(\mathbf{x}, t)$ over the domains U_1 (b) and U_{30} (d).

For an arbitrary length parameter $a > 0$, we consider square-shaped flow domains of the form $U_a = \{(x, y) \in \mathbb{R}^2 : (x, y) \in [-a, a]^2\}$, on which to find the deformation velocity component $\mathbf{v}_d(\mathbf{x}, t)$ of (33). As our optimization problem (9) was posed for three-dimensional velocity fields, we formally extend (33) with an identically zero velocity component in the z -direction. As a result, the angular velocity vector $\boldsymbol{\omega}$, defined by (14), will only have a single nonzero component, $\boldsymbol{\omega} = (\boldsymbol{\omega})_z$. In this simple example, an analytic computation of $\boldsymbol{\omega}$ is possible, yielding $\boldsymbol{\omega} = -2$.

In Fig. 1a, we show the streamlines of system (33) for the time instant $t = 0$ (other time instants yield similar streamlines) over the domain U_1 . In Fig. 1b, we show the instantaneous streamlines of the deformation velocity field \mathbf{v}_d obtained from formulas (6)–(7) over U_1 . In Fig. 1c–d, we again show the original and deformation streamlines for the larger domain U_{30} .

The streamline structure of the original velocity field (33) suggests a vortical region around the origin, which is also the prediction of all classic, frame-dependent vortex criteria when applied to this example. In contrast, Pedergrana et al. [51] show that the origin is a saddle-type LCS residing in a hyperbolic region that exhibits chaotic mixing. This behavior makes (33) a false positive of the traditional vortex criteria. In spite of this, instantaneous streamlines of the deformation velocity correctly reveal the saddle type of the origin, as seen in Fig. 1b. We recall that the instantaneous streamlines have generally no direct connection with the Lagrangian dynamics in an unsteady flow and this fact remains true for the deformation velocity \mathbf{v}_d as well. Yet, in

this example, the objective streamlines of \mathbf{v}_d correctly reflect the Lagrangian stability properties of the origin.

Our second example, taken from the same class of explicit Navier–Stokes solutions as (33), is the velocity field

$$\mathbf{v}(\mathbf{x}, t) = \begin{pmatrix} \dot{x} \\ \dot{y} \end{pmatrix} = \begin{pmatrix} \sin 4t & \cos 4t + \frac{1}{2} \\ \cos 4t - \frac{1}{2} & -\sin 4t \end{pmatrix} \begin{pmatrix} x \\ y \end{pmatrix} - 0.015 \begin{pmatrix} x^2 - y^2 \\ -2xy \end{pmatrix}. \tag{34}$$

In [51], (34) is shown to be a false negative for all available frame-dependent vortex criteria. Indeed, the instantaneous streamlines indicate a saddle-type structure near the origin, yet the Lagrangian particle motion is quasiperiodic (elliptic). In Fig. 2, we show the streamlines of the velocity field (34), along with the streamlines of its deformation component, which has $\boldsymbol{\omega} = -\frac{1}{2}$. This time, the streamlines of the deformation component have the same structure as those of the original velocity field. In Fig. 2c, we show the velocity field, as observed from the frame co-rotating with the closest rigid body velocity. This is calculated by solving for $\mathbf{Q}_{RB}(t)$ according to (25). In this case, the solution can be written out explicitly,

$$\mathbf{Q}_{RB}(t) = \begin{pmatrix} \cos \omega t & -\sin \omega t \\ \sin \omega t & \cos \omega t \end{pmatrix},$$

as noted for two-dimensional flows in [28]. The velocity field observed in the frame co-rotating with $\mathbf{v}_{RB}(\mathbf{x}, t)$ is (28). The trajectories of $\mathbf{Q}_{RB}^T(t)\mathbf{v}_d(\mathbf{x}, t)$ are indeed topologically equivalent to those

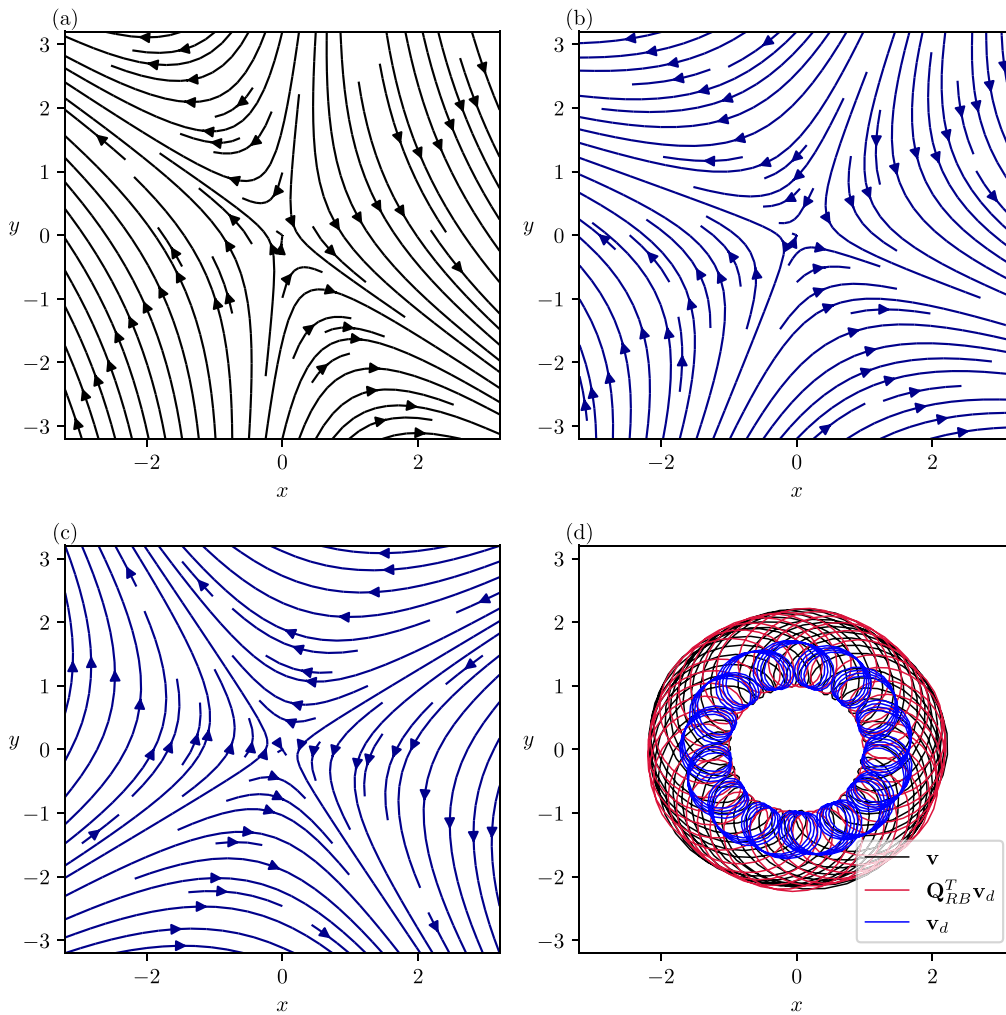


Fig. 2. The velocity field (34) and its deformation velocity component. (a) Streamlines of (34) at time $t = 10$. Panel (b) shows the streamlines of the deformation component \mathbf{v}_d , while panel (c) shows the streamlines of the observed velocity, $\mathbf{Q}_{RB}^T(t)\mathbf{v}_d$. In panel (d), a trajectory of the velocity field \mathbf{v} is shown in black. The corresponding trajectory of the deformation component, \mathbf{v}_d , (of the observed velocity, $\mathbf{Q}_{RB}^T(t)\mathbf{v}_d$) is shown in blue (red). (For interpretation of the references to color in this figure legend, the reader is referred to the web version of this article.)

of \mathbf{v} . This is illustrated in Fig. 2d, where a trajectory of \mathbf{v} is shown together with the corresponding trajectory of $\mathbf{Q}_{RB}^T(t)\mathbf{v}_d(\mathbf{x}, t)$.

Our third example is a kinematic velocity model describing an unsteady gyre in a rotating circular tank, with free slip boundary conditions along the tank wall [52]. This unsteady flow develops Lagrangian flow separation and reattachment, exhibited by a sharp material spike emanating from the boundary and hitting the boundary again at a diametrically opposite point. This separation and reattachment, however, have no indication in the Eulerian frame as all streamlines remain circular for all times (see Fig. 3a). Although Lekien and Haller [52] show that the Lagrangian separation does not occur at instantaneous stagnation points on the boundary, such points often serve as rough indicators of flow separation [53]. Their absence, therefore, suggests a lack of flow separation even though that is not the case here.

The two-dimensional model velocity field in [52] has the stream function

$$\Psi(\mathbf{x}, t) = (|\mathbf{x}|^2 - 1)(x \sin \omega_s t + y \cos \omega_s t) - \frac{1}{2} \omega_s |\mathbf{x}|^2. \quad (35)$$

Our physical domain is the rotating circular container, i.e., $U = \{(x, y) \in \mathbb{R}^2 : x^2 + y^2 \leq 1\}$, on which we recover the rigid body angular velocity $\omega = \omega_s$, as anticipated. In Fig. 3b, we show the instantaneous streamlines of the deformation velocity \mathbf{v}_d at the same time instant that we used for plotting

the streamlines of \mathbf{v} in Fig. 3a. We note the appearance of two, diametrically opposite stagnation points for \mathbf{v}_d along the boundary, correctly suggesting the simultaneous presence of separation and reattachment in the flow.

As a fourth example, we illustrate the calculation of the deformation velocity field on a two-dimensional unsteady velocity data set from AVISO satellite altimetry measurements [54]. We work with a single velocity snapshot from April 12, 2014. The domain of the dataset is the Gulf Stream region. The velocity field is obtained from the sea surface height (SSH), which is the stream function of the surface velocity field under the geostrophic assumption.

By choosing the domain to be too large, we might include regions in which multiple eddies coexist. To highlight this dependence of \mathbf{v}_d on the domain of interest, we perform the $\mathbf{v} = \mathbf{v}_{RB} + \mathbf{v}_d$ decomposition of the surface velocity field over two different domains. First, we select the full domain $U = [290^\circ, 310^\circ] \times [33^\circ, 41^\circ]$ in longitude–latitude coordinates. In this case, we obtain the small, negative value $\omega = -0.0037$. In contrast, if we choose U around an Eulerian mesoscale eddy highlighted in Fig. 4b, then $\omega = 0.6995$ is a considerably larger positive number, indicative of the closest rigid body rotation well describing the eddy. This was to be expected since the full observed region appears to contain several rotating features and hence lacks a single dominant rigid-body rotation component. Indeed, a comparison of Fig. 4a and Fig. 4b confirms that the

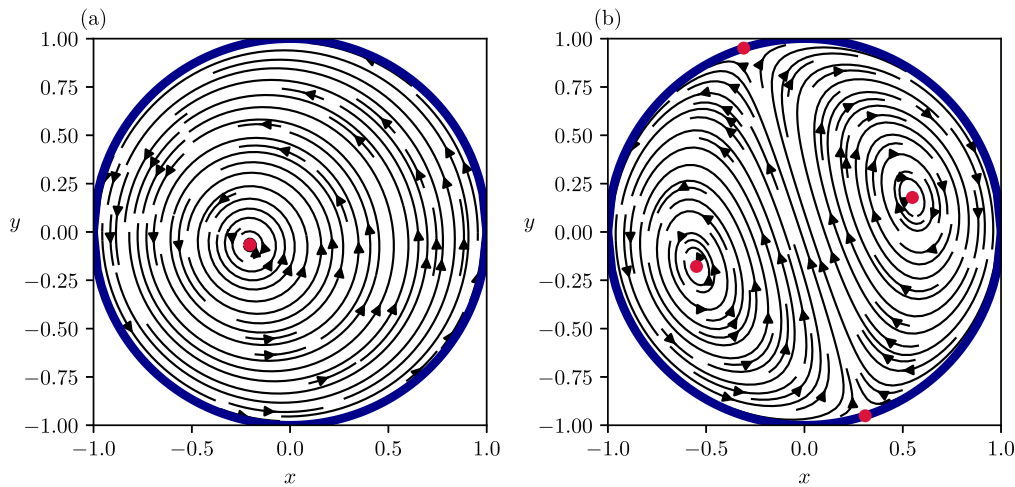


Fig. 3. Streamlines of the kinematic model (35) (a) and those of its deformation velocity component (b). The boundary of the domain U is shown in blue, while red points denote the stagnation points in the flow. For both panels, $t = \pi/10$. The rigid body angular velocity is $\omega = \omega_s = 4$. (For interpretation of the references to color in this figure legend, the reader is referred to the web version of this article.)

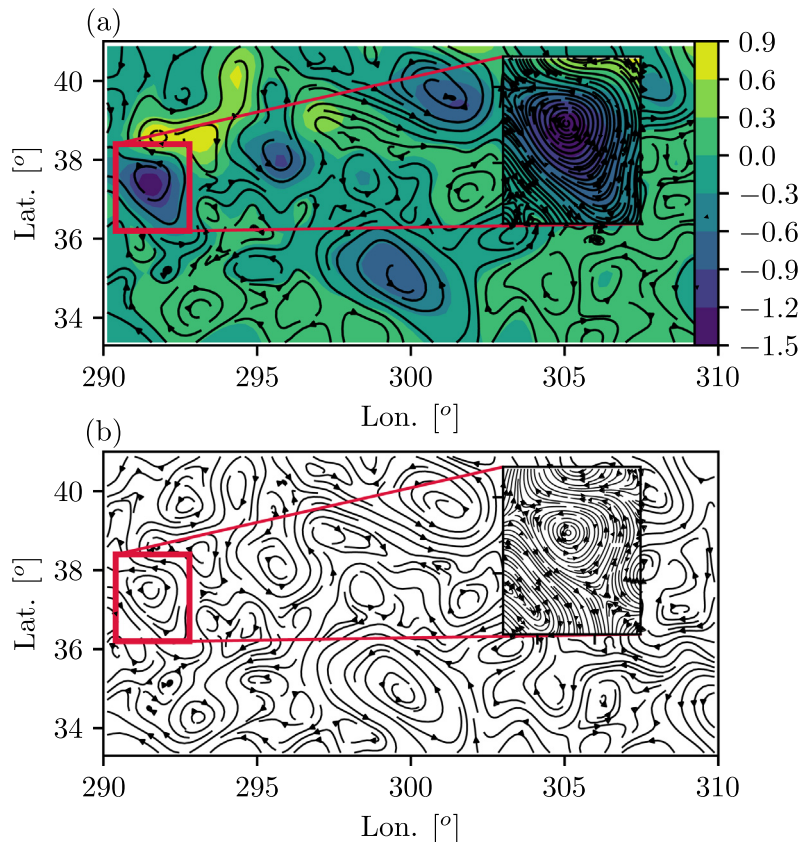


Fig. 4. The AVISO velocity field and its objective deformation component on April 12, 2014. (a) The original streamlines overlaid on the sea surface height (SSH) field measured in meters. The inset shows a smaller subdomain encircling a mesoscale eddy. (b): objective streamlines of the deformation velocity \mathbf{v}_d . The inset in (b) shows the streamlines of the deformation component calculated from the small region around the eddy.

subtraction of the rigid body velocity field does not alter the structure of the streamlines considerably on this large domain. As a result, the objectivized scalar fields such as the kinetic energy would also be practically indistinguishable from those evaluated on the original velocity field.

For practical purposes, this means that when working with velocity fields coming from models or observations that cover a large domain of the globe, one has to first isolate smaller regions

of interest. Otherwise, for large domains, the principle outlined here returns that there is no single co-moving observer and we have $\mathbf{v}_{RB} \approx 0$.

In contrast, the velocity field in the region around the eddy of Fig. 4a is expected to have a dominant rigid-body component. This is consistent with the observations of Tél et al. [55], who showed experimentally that the core of a vortex approximately rotates as a rigid body. Nevertheless, we find that the deformation

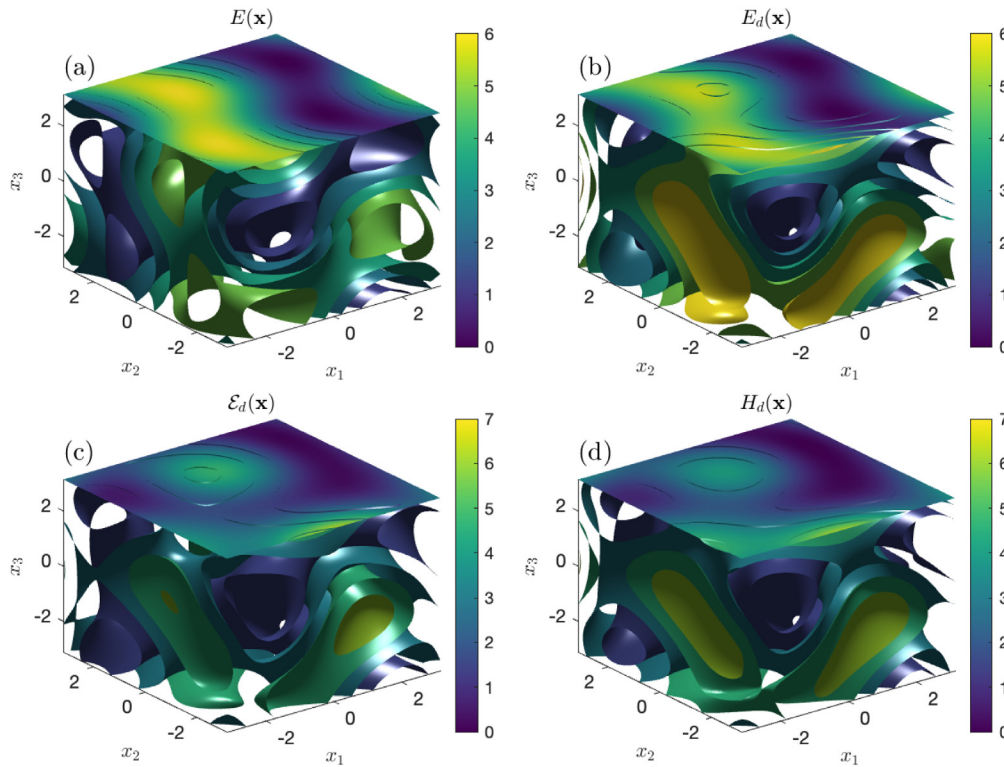


Fig. 5. Energy, enstrophy and helicity isosurfaces for the ABC flow. In panel (a), isosurfaces of the energy $E = \frac{1}{2}|\mathbf{v}(\mathbf{x}, t)|^2$ are shown for the velocity field (36), with parameters $A = \sqrt{3}$, $B = \sqrt{2}$, $C = 1$. These coincide with isosurfaces of both $\frac{1}{2}\mathcal{E} = \frac{1}{2}|\nabla \times \mathbf{v}|^2$ and $\frac{1}{2}H = \frac{1}{2}|\mathbf{v} \cdot \nabla \times \mathbf{v}|^2$. Panel (b) shows isosurfaces of the deformation kinetic energy $E_d = \frac{1}{2}|\mathbf{v}_d(\mathbf{x}, t)|^2$. In panels (c) and (d), isosurfaces of the deformation enstrophy, $\frac{1}{2}\mathcal{E}_d = \frac{1}{2}|\nabla \times \mathbf{v}_d|^2$ and the deformation helicity, $\frac{1}{2}H_d = \frac{1}{2}|\mathbf{v}_d \cdot \nabla \times \mathbf{v}_d|^2$ are shown, respectively. The deformation velocity field $\mathbf{v}_d(\mathbf{x}, t)$ is given as $\mathbf{v}_d(\mathbf{x}, t) = \mathbf{v}(\mathbf{x}, t) - \boldsymbol{\omega} \times \mathbf{x}$, where \mathbf{v} and $\boldsymbol{\omega}$ are defined in (36) and (37).

component is still nonzero. The inset of Fig. 4b shows the streamlines of the deformation component computed with respect to this eddy.

4.2. Objectivized Eulerian fields in 3D

We now discuss the following objectivized Eulerian scalar fields: the deformation kinetic energy $E_d(\mathbf{x})$, the deformation enstrophy $\mathcal{E}_d(\mathbf{x})$, and the deformation helicity $H_d(\mathbf{x})$ defined in (29). We calculate them for the classic ABC velocity field [56], given by

$$\mathbf{v}(\mathbf{x}, t) = \begin{pmatrix} \dot{x}_1 \\ \dot{x}_2 \\ \dot{x}_3 \end{pmatrix} = \begin{pmatrix} A \sin x_3 + C \cos x_2 \\ B \sin x_1 + A \cos x_3 \\ C \sin x_2 + B \cos x_1 \end{pmatrix}. \quad (36)$$

We take the domain $U = [-\pi, \pi]^3$ for the calculation of the deformation component. After applying formula (14), we obtain

$$\bar{\mathbf{x}} = \mathbf{0}, \quad \bar{\mathbf{v}} = \mathbf{0}, \quad \boldsymbol{\omega} = \frac{3}{2\pi^2} \begin{pmatrix} C \\ A \\ B \end{pmatrix}, \quad (37)$$

yielding the deformation velocity

$$\mathbf{v}_d = \begin{pmatrix} A \sin x_3 + C \cos x_2 \\ B \sin x_1 + A \cos x_3 \\ C \sin x_2 + B \cos x_1 \end{pmatrix} - \frac{3}{2\pi^2} \begin{pmatrix} Bx_2 - Ax_3 \\ Cx_3 - Bx_1 \\ Ax_1 - Cx_2 \end{pmatrix}.$$

In Fig. 5, we show level sets of the energy, half the enstrophy, and half the helicity of the ABC flow with the classic choice of parameters $A = \sqrt{3}$, $B = \sqrt{2}$, $C = 1$, which results in chaotic Lagrangian dynamics [56]. For comparisons, we also show the objectivized versions of the same quantities, calculated from the deformation velocity (7), with $\boldsymbol{\omega}$ given by (37). Since for the ABC

flow, $\mathbf{v} \equiv \nabla \times \mathbf{v}$, the classic enstrophy and the helicity are equal to twice the energy. This, however, is no longer the case for the deformation velocity, for which we have

$$\nabla \times \mathbf{v}_d = \nabla \times \mathbf{v} - \nabla \times (\boldsymbol{\omega} \times \mathbf{x}) = \mathbf{v} - 2\boldsymbol{\omega}.$$

As a consequence, the deformation kinetic energy is not proportional to either the deformation enstrophy or the deformation helicity. In addition, the latter three quantities are objective scalar fields while their counterparts, E , \mathcal{E} , and H depend on the observer.

To illustrate the objectivity of the deformation kinetic energy E_d , we transform the velocity field (36) to a frame rotating around the z -axis with a constant angular velocity $\omega_r = 5$, defined by $\mathbf{x} = \mathbf{Q}(t)\mathbf{y}$, where

$$\mathbf{Q}(t) = \begin{pmatrix} \cos \omega_r t & -\sin \omega_r t & 0 \\ \sin \omega_r t & \cos \omega_r t & 0 \\ 0 & 0 & 1 \end{pmatrix}. \quad (38)$$

The velocity of the ABC flow observed in the \mathbf{y} -frame is then

$$\dot{\mathbf{y}} = \hat{\mathbf{v}}(\mathbf{y}, t) = \mathbf{Q}^T(t) (\mathbf{v}(\mathbf{Q}(t)\mathbf{y}) - \dot{\mathbf{Q}}(t)\mathbf{y}). \quad (39)$$

After substituting (36) and the expression for $\mathbf{Q}(t)$ into the transformation formula (39), we obtain an explicitly time dependent velocity field $\hat{\mathbf{v}}(\mathbf{y}, t)$. As discussed in Section 3.2.2, we then apply the formulas (6) and (7) to calculate the deformation velocity $\hat{\mathbf{v}}_d(\mathbf{y}, t)$ in the \mathbf{y} -frame. In Fig. 6, we show the kinetic energies E and \hat{E} calculated in the \mathbf{x} - and \mathbf{y} -frames, respectively, along with their deformation counterparts, E_d and \hat{E}_d .

When observed from the frame defined by (38), the kinetic energy $\hat{E} = \frac{1}{2}|\hat{\mathbf{v}}(\mathbf{y}, t)|^2$ has explicit time dependence. As Fig. 6b and Fig. 6c show, the isosurfaces of the kinetic energy outline a vortical structure parallel to the z -axis, the rotational axis of

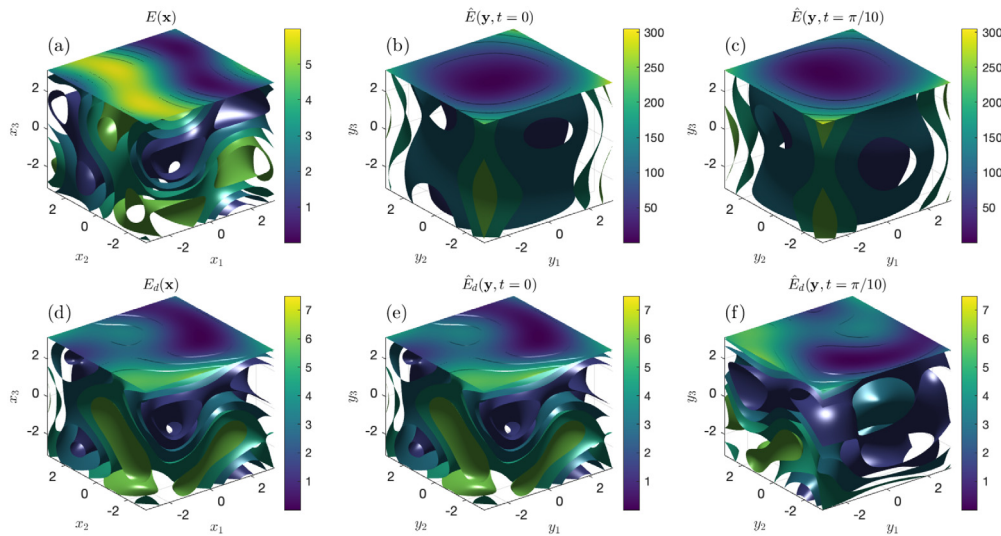


Fig. 6. The kinetic energy E and deformation kinetic energy E_d of the ABC flow observed in different frames. In panel (a), isosurfaces of the energy $E = \frac{1}{2}|\mathbf{v}(\mathbf{x}, t)|^2$ are shown for the velocity field (36), with parameters $A = \sqrt{3}$, $B = \sqrt{2}$, $C = 1$. In panels (b) and (c) the isosurfaces of the transformed kinetic energy, $\widehat{E} = \frac{1}{2}|\widehat{\mathbf{v}}(\mathbf{y}, t)|^2$, are shown for $t = 0$ and $t = \pi/10$. The transformation between the \mathbf{x} and \mathbf{y} frames is $\mathbf{x} = \mathbf{Q}(t)\mathbf{y}$, with $\mathbf{Q}(t)$ given by (38). Coordinates in the \mathbf{y} -frame are labeled as (y_1, y_2, y_3) . In panel (d) the isosurfaces of the deformation kinetic energy $E_d(\mathbf{x})$ are shown, while panels (e)–(f) show the isosurfaces of $\widehat{E}_d(\mathbf{y}, t)$, the deformation kinetic energy computed in the \mathbf{y} -frame for $t = 0$ and $t = \pi/10$.

the \mathbf{y} -frame. In contrast, the deformation kinetic energy preserves the topology of its isosurfaces, regardless of which frame it is observed in. Comparing the isosurfaces of the deformation kinetic energy in the \mathbf{x} and \mathbf{y} frames, shown in Fig. 6d–f, the only difference is that for $t \neq 0$, due to the frame change, the whole computational domain is rotated around the z -axis according to $\mathbf{y} = \mathbf{Q}^T(t)\mathbf{x}$. Otherwise, the topologies of E_d and \widehat{E}_d are identical in each case.

5. Conclusion

We have derived a decomposition of an arbitrary velocity field \mathbf{v} on a domain U into its closest rigid body component, \mathbf{v}_{RB} , and a deformation component, $\mathbf{v}_d = \mathbf{v} - \mathbf{v}_{RB}$. The distance between \mathbf{v} and \mathbf{v}_{RB} is minimal in the L^2 norm.

We have explicitly solved the optimization problem (11) for the angular velocity vector $\boldsymbol{\omega}$ of the rigid body motion, which can equivalently be expressed with a skew-symmetric tensor $\boldsymbol{\Omega}$. This unique rigid-body component renders the deformation component objective and physically observable. Observability means that there is a distinguished Euclidean observer who measures the velocity field to be equal to its deformation component.

We have illustrated the calculation of the deformation velocity on examples. In particular, for planar flows, we have used unsteady, polynomial solutions of the Navier–Stokes equation, a kinematic model exhibiting material separation, and a satellite velocimetry data set of the ocean surface velocity as examples. We have computed the instantaneous deformation streamlines and compared the trajectories of the deformation component to those of the original velocity field.

With the help of the deformation velocity, we can also objectivize most Eulerian quantities typically used in flow analysis just by computing them on \mathbf{v}_d . This is equivalent to computing these Eulerian quantities on the full velocity field \mathbf{v} but in a frame co-moving with \mathbf{v}_{RB} . We have illustrated the objectivity of the deformation kinetic energy, deformation enstrophy and deformation helicity for the classic ABC flow by recomputing these quantities in a rotating frame. While the level set structure of the kinetic energy changes substantially when observed from the rotating frame, the deformation kinetic energy is indeed indifferent to this observer change.

In almost all the examples considered here, the computation of the deformation velocity field was simple and explicit. In some cases, the deformation velocity provided more insight into the flow, in some cases it did not. This is because truly unsteady, spatially complex flows do not have a unique distinguished frame [9]. We argue, however, that the variational problem we have posed and solved here explicitly provides the closest possible rigid-body frame in a well-defined physical sense.

Declaration of competing interest

The authors declare that they have no known competing financial interests or personal relationships that could have appeared to influence the work reported in this paper.

Data availability

Numerical implementation of the proposed method (Original data) (Private repository)

Acknowledgments

The altimeter products were processed by SSALTO/DUACS and distributed by AVISO+ (<https://www.aviso.altimetry.fr>) with support from CNES. We acknowledge support from the Turbulent Superstructures Program (SPP1881) of the German National Science Foundation (DFG).

Appendix A. The derivative of $L_1(\boldsymbol{\Omega}, t)$

To find the extremum of the functional $\widetilde{L}_1(\boldsymbol{\Omega}, t)$ in Eq. (12), we first express it in terms of the angular velocity $\boldsymbol{\omega}$. The relationship

$$\boldsymbol{\Omega}(t)\mathbf{e} = \boldsymbol{\omega}(t) \times \mathbf{e}, \quad \forall \mathbf{e} \in \mathbb{R}^3,$$

translates to coordinate components as

$$\boldsymbol{\Omega}_{ij}e_j = \varepsilon_{ijk}\omega_j e_k, \tag{40}$$

where ε_{ijk} is the Levi-Civita symbol. Substituting (40) into (12), we obtain

$$\widetilde{L}_1(\boldsymbol{\omega}, t) = \frac{1}{M} \int_U \left\{ -2(\mathbf{v}_i - \dot{\mathbf{x}}_i)\varepsilon_{ijk}\omega_j (\mathbf{x}_k - \bar{\mathbf{x}}_k) \right\} \tag{41}$$

$$+ \varepsilon_{ijk}\omega_j (\mathbf{x}_k - \bar{\mathbf{x}}_k) \varepsilon_{ilm}\omega_l (\mathbf{x}_m - \bar{\mathbf{x}}_m) \} \rho(\mathbf{x}, t)dV.$$

We now seek the minimizer $\omega(t)$ as the solution to the system of three equations

$$\frac{\partial}{\partial \omega_n} \tilde{L}_1(\omega, t) = 0, \quad n = 1, 2, 3. \tag{42}$$

We then differentiate the integrand in (41) to obtain

$$\begin{aligned} & \frac{\partial}{\partial \omega_n} \left\{ -2(\mathbf{v}_i - \dot{\bar{\mathbf{x}}}_i)\varepsilon_{ijk}\omega_j (\mathbf{x}_k - \bar{\mathbf{x}}_k) \right. \\ & \left. + \varepsilon_{ijk}\omega_j (\mathbf{x}_k - \bar{\mathbf{x}}_k) \varepsilon_{ilm}\omega_l (\mathbf{x}_m - \bar{\mathbf{x}}_m) \right\} \\ &= -2\varepsilon_{nki}(\mathbf{v}_i - \dot{\bar{\mathbf{x}}}_i)(\mathbf{x}_k - \bar{\mathbf{x}}_k) + 2\omega_n(\mathbf{x}_m - \bar{\mathbf{x}}_m)^2 \\ & \quad - 2\omega_k(\mathbf{x}_k - \bar{\mathbf{x}}_k)(\mathbf{x}_n - \bar{\mathbf{x}}_n). \end{aligned} \tag{43}$$

Written in coordinate-invariant form, Eq. (43) becomes

$$-2(\mathbf{x} - \bar{\mathbf{x}}) \times (\mathbf{v} - \dot{\bar{\mathbf{x}}}) + 2(|\mathbf{x} - \bar{\mathbf{x}}|^2)\omega - 2(\mathbf{x} - \bar{\mathbf{x}}) \otimes (\mathbf{x} - \bar{\mathbf{x}})\omega.$$

Substituting this derivative of the integrand into (42) and dividing by 2, we obtain Eq. (13), as claimed.

Appendix B. The second derivative of $\tilde{L}_1(\Omega, t)$

To compute the Hessian of the function $\tilde{L}_1(\Omega, t)$, we start from (41). Taking the derivative of the integrand with respect to ω_n , we have already obtained the expression (43). Further differentiation with respect to ω_p then yields

$$\begin{aligned} & \frac{\partial}{\partial \omega_p} \left[2\varepsilon_{ink}(\mathbf{v}_i - \dot{\bar{\mathbf{x}}}_i)(\mathbf{x}_k - \bar{\mathbf{x}}_k) + 2\omega_n(\mathbf{x}_m - \bar{\mathbf{x}}_m)^2 \right. \\ & \left. - 2\omega_k(\mathbf{x}_k - \bar{\mathbf{x}}_k)(\mathbf{x}_n - \bar{\mathbf{x}}_n) \right] \\ &= 2\delta_{np}(\mathbf{x}_m - \bar{\mathbf{x}}_m)^2 - 2(\mathbf{x}_p - \bar{\mathbf{x}}_p)(\mathbf{x}_n - \bar{\mathbf{x}}_n). \end{aligned}$$

Expressed in a coordinate-invariant form, we therefore obtain the Hessian

$$\frac{\partial^2}{\partial \omega_n \partial \omega_p} \tilde{L}_1(\omega, t) = 2\delta_{np}(\mathbf{x}_m - \bar{\mathbf{x}}_m)^2 - 2(\mathbf{x}_p - \bar{\mathbf{x}}_p)(\mathbf{x}_n - \bar{\mathbf{x}}_n) = \frac{2}{M} [\Theta]_{np},$$

as claimed.

Appendix C. Transformation rule for the closest rigid-body angular velocity vector

Under a Euclidean frame change (15), the velocity $\mathbf{v}(\mathbf{x}, t)$ and the average velocity $\bar{\mathbf{v}}(t)$ transform as

$$\begin{aligned} \hat{\mathbf{v}} &= \mathbf{Q}^T (\mathbf{v} - \dot{\mathbf{Q}}\mathbf{y} - \dot{\mathbf{b}}), \\ \hat{\bar{\mathbf{v}}} &= \mathbf{Q}^T (\bar{\mathbf{v}} - \dot{\mathbf{Q}}\bar{\mathbf{y}} - \dot{\bar{\mathbf{b}}}). \end{aligned} \tag{44}$$

Since $\mathbf{Q}^T \dot{\mathbf{Q}}$ is skew-symmetric, it has a dual vector associated to it, $\dot{\mathbf{q}}$, defined as

$$\dot{\mathbf{Q}}\mathbf{Q}^T \mathbf{e} = \dot{\mathbf{q}} \times \mathbf{e} \quad \forall \mathbf{e} \in \mathbb{R}^3. \tag{45}$$

Substituting the transformation rules (19), (44) into (13), we obtain

$$\begin{aligned} \hat{\Theta} \hat{\omega} &= M(\mathbf{y} - \bar{\mathbf{y}}) \times (\hat{\mathbf{v}} - \hat{\bar{\mathbf{v}}}) \\ &= M\overline{\mathbf{Q}^T(\mathbf{x} - \bar{\mathbf{x}}) \times \mathbf{Q}^T(\mathbf{v} - \bar{\mathbf{v}} - \dot{\mathbf{Q}}\mathbf{Q}^T(\mathbf{x} - \bar{\mathbf{x}}))}. \end{aligned} \tag{46}$$

We now recall that for any rotation matrix \mathbf{Q} and for arbitrary vectors \mathbf{a} and \mathbf{b} , we have $\mathbf{Q}\mathbf{a} \times \mathbf{Q}\mathbf{b} = \mathbf{Q}(\mathbf{a} \times \mathbf{b})$. Furthermore, for

any three vectors $\mathbf{a}, \mathbf{b}, \mathbf{c} \in \mathbb{R}^3$, we have $\mathbf{a} \times (\mathbf{b} \times \mathbf{c}) = \mathbf{b}(\mathbf{a} \cdot \mathbf{c}) - \mathbf{c}(\mathbf{a} \cdot \mathbf{b})$. With these identities, we can rewrite Eq. (46) as

$$\begin{aligned} \hat{\Theta} \hat{\omega} &= M\overline{\mathbf{Q}^T(\mathbf{x} - \bar{\mathbf{x}}) \times (\mathbf{v} - \bar{\mathbf{v}} - \dot{\mathbf{Q}}\mathbf{Q}^T(\mathbf{x} - \bar{\mathbf{x}}))} \\ &= M\overline{\mathbf{Q}^T(\mathbf{x} - \bar{\mathbf{x}}) \times (\mathbf{v} - \bar{\mathbf{v}}) - \dot{\mathbf{q}}|\mathbf{x} - \bar{\mathbf{x}}|^2 + (\mathbf{x} - \bar{\mathbf{x}}) [\dot{\mathbf{q}} \cdot (\mathbf{x} - \bar{\mathbf{x}})]} \\ &= M\overline{\mathbf{Q}^T(\mathbf{x} - \bar{\mathbf{x}}) \times (\mathbf{v} - \bar{\mathbf{v}}) - \mathbf{Q}^T \Theta \dot{\mathbf{q}}} \\ &= M\mathbf{Q}^T \left[\frac{1}{M} \Theta \omega - \frac{1}{M} \Theta \dot{\mathbf{q}} \right]. \end{aligned}$$

$$\mathbf{Q}^T \Theta \mathbf{Q} \hat{\omega} = \mathbf{Q}^T \Theta \omega - \mathbf{Q}^T \Theta \dot{\mathbf{q}}$$

Substituting the transformation formula (19) for the tensor $\hat{\Theta}$ into the left-hand side of this last equation then yields the transformation formula

$$\hat{\omega} = \mathbf{Q}^T (\omega - \dot{\mathbf{q}})$$

for the angular velocity ω .

Appendix D. Transformation rule of the deformation velocity

Under a Euclidean frame change (15), the deformation velocity field $\mathbf{v}_d(\mathbf{x}, t)$ defined in (7) can be computed in the \mathbf{y} -frame as

$$\begin{aligned} \hat{\mathbf{v}}_d &= \hat{\mathbf{v}} - \hat{\bar{\mathbf{v}}} - \hat{\omega} \times (\mathbf{y} - \bar{\mathbf{y}}) \\ &= \mathbf{Q}^T [\mathbf{v} - \bar{\mathbf{v}} - \dot{\mathbf{Q}}\mathbf{Q}^T(\mathbf{x} - \bar{\mathbf{x}})] - \mathbf{Q}^T (\omega - \dot{\mathbf{q}}) \times \mathbf{Q}^T(\mathbf{x} - \bar{\mathbf{x}}) \\ &= \mathbf{Q}^T [\mathbf{v} - \bar{\mathbf{v}} - \omega \times (\mathbf{x} - \bar{\mathbf{x}})] \\ &= \mathbf{Q}^T \mathbf{v}_d, \end{aligned} \tag{47}$$

which proves the objectivity of $\mathbf{v}_d(\mathbf{x}, t)$.

Appendix E. The full velocity field in a frame co-moving with \mathbf{v}_{RB}

Under the observer change defined in (24)–(25), the transformed velocity field becomes

$$\begin{aligned} \hat{\mathbf{v}} &= \mathbf{Q}_{RB}^T (\mathbf{v} - \dot{\mathbf{Q}}_{RB}\mathbf{y} - \dot{\mathbf{b}}_{RB}) \\ &= \mathbf{Q}_{RB}^T (\mathbf{v} - \dot{\mathbf{Q}}_{RB}\mathbf{Q}_{RB}^T(\mathbf{x} - \mathbf{b}_{RB}) - \dot{\mathbf{b}}_{RB}) \\ &= \mathbf{Q}_{RB}^T (\mathbf{v} - \omega \times \mathbf{x} + \omega \times \bar{\mathbf{x}} - \bar{\mathbf{v}}) = \mathbf{Q}_{RB}^T \mathbf{v}_d = \hat{\mathbf{v}}_d, \end{aligned}$$

where we have used formula (47).

Appendix F. Deformation velocity of the deformation velocity

First, as a special case, we formally calculate ω for a rigid-body velocity field

$$\mathbf{v}(\mathbf{x}, t) = \mathbf{p} \times (\mathbf{x} - \bar{\mathbf{x}}) + \bar{\mathbf{v}}. \tag{48}$$

Noting that

$$\begin{aligned} (\mathbf{x} - \bar{\mathbf{x}}) \times (\mathbf{v} - \bar{\mathbf{v}}) &= (\mathbf{x} - \bar{\mathbf{x}}) \times \mathbf{p} \times (\mathbf{x} - \bar{\mathbf{x}}) \\ &= |\mathbf{x} - \bar{\mathbf{x}}|^2 \mathbf{p} + (\mathbf{x} - \bar{\mathbf{x}}) \otimes (\mathbf{x} - \bar{\mathbf{x}})\mathbf{p}, \end{aligned}$$

we find from (14) that

$$\begin{aligned} \omega &= M \Theta^{-1} \left[|\mathbf{x} - \bar{\mathbf{x}}|^2 \mathbf{p} + (\mathbf{x} - \bar{\mathbf{x}}) \otimes (\mathbf{x} - \bar{\mathbf{x}})\mathbf{p} \right] \\ &= M \Theta^{-1} \frac{1}{M} \Theta \mathbf{p} = \mathbf{p}, \end{aligned} \tag{49}$$

i.e., ω coincides with the angular velocity of the rigid body.

Therefore, noting that (14) shows ω to be a homogeneous linear function of the velocity field \mathbf{v} , we obtain

$$\omega^{(2)} = \omega - \omega = \mathbf{0}.$$

In other words, the deformation velocity has a vanishing closest rigid body component under our optimization principle, given that we also have $\mathbf{v}(\bar{\mathbf{x}}, t) = \bar{\mathbf{v}}$ in Eq. (48).

Appendix G. Generalizing the objective function

As a straightforward generalization to the mass-based L^2 norm (1), we consider here the following family of Sobolev norms to measure the closeness of two velocity fields:

$$\|\mathbf{f}\|_{H^k}^2 = \frac{1}{M} \int_U |\mathbf{f}(\mathbf{x}, t)|^2 dm + \alpha \frac{1}{M} \int_U |\mathbf{D}_x \mathbf{f}(\mathbf{x}, t)|^2 dm \quad (50)$$

$$+ \frac{1}{M} \sum_{i=2}^k \beta_i \int_U |\mathbf{D}_x^i \mathbf{f}(\mathbf{x}, t)|^2 dm. \quad (51)$$

This H^k norm is defined for integrable functions over U whose derivatives up to order k are also integrable. The constants $\alpha, \beta_i \geq 0$ ensure the same physical dimension for all terms in $\|\mathbf{f}\|_{H^k}^2$ and also serve to assign different weights to the different spatial scales in $\mathbf{f}(\mathbf{x}, t)$. Specifically, $\alpha = \beta_1 = \dots = \beta_k = 0$ eliminates the consideration of smaller scales in the norm of $\mathbf{f}(\mathbf{x}, t)$, whereas $\alpha, \beta_i \rightarrow \infty$ gives full weight to the smaller scales.

Therefore, the objective function to be minimized becomes

$$L_{H^k}(\Omega, \mathbf{x}_A, t) = \|\mathbf{v}(\mathbf{x}, t) - \mathbf{v}_{RB}(\mathbf{x}, t)\|_{H^k}^2. \quad (52)$$

Due to the spatial linearity of \mathbf{v}_{RB} , for any $k \geq 1$, extrema of $L_{H^k}(\Omega(t), t)$ are defined by the equation

$$\frac{\partial}{\partial \Omega} L_{H^k}(\Omega, t) \equiv \frac{\partial}{\partial \Omega} L_{H^1}(\Omega, t) = 0. \quad (53)$$

Therefore, the weights given to the higher-order derivatives in (51) can be set as $\beta_1 = \dots = \beta_k = 0$ without loss of generality. Therefore, the only remaining parameter to determine is the weight of the derivative term, α .

With a simple extension of the derivation outlined in Section 3, the closest rigid-body angular velocity with respect to the H^1 norm is

$$\omega_\alpha = M \Theta_\alpha^{-1} (\mathbf{x} - \bar{\mathbf{x}}) \times (\mathbf{v} - \bar{\mathbf{v}}) + \alpha \nabla \times \mathbf{v}, \quad (54)$$

where the moment of inertia tensor Θ_0 is modified to $\Theta_\alpha = \Theta_0 + 2\alpha \mathbf{I}$.

In Fig. 7, we compare the optimal rigid-body angular velocity for various values of α . We take the AVISO dataset analyzed in Fig. 4 and compute ω again. For both of the domains considered, we see that ω_α does not change significantly with α . Therefore, the basic conclusions we drew from the $\alpha = 0$ result of Fig. 4 extends to any α . Optimizing over the whole domain gives small negative values of the angular velocity, while optimizing over the neighborhood of the mesoscale eddy gives a larger positive angular velocity. In light of this, the resulting deformation velocities are also similar to each other for non-zero values of α . In the main body of this paper, we have decided to set $\alpha = 0$ in the main results to remain in line with our physical motivation.

References

[1] A.E. Perry, M.S. Chong, Topology of flow patterns in vortex motions and turbulence, *Appl. Sci. Res.* 53 (1994) 357–374.
 [2] G. Haller, An objective definition of a vortex, *J. Fluid Mech.* 525 (2005) 1–26.
 [3] G. Haller, A. Hadjighasem, M. Farazmand, F. Huhn, Defining coherent vortices objectively from the vorticity, *J. Fluid Mech.* 795 (2016) 136–173.
 [4] M.E. Gurtin, *An Introduction to Continuum Mechanics*, Academic Press, 1981.
 [5] L.D. Landau, E.M. Lifshitz, *The Classical Theory of Fields*, Pergamon, 1975.
 [6] F. Waleffe, Exact coherent structures in channel flow, *J. Fluid Mech.* 435 (2001) 93–102.
 [7] F. Mellibovsky, B. Eckhardt, From travelling waves to mild chaos: a supercritical bifurcation cascade in pipe flow, *J. Fluid Mech.* 709 (2012) 149–190.

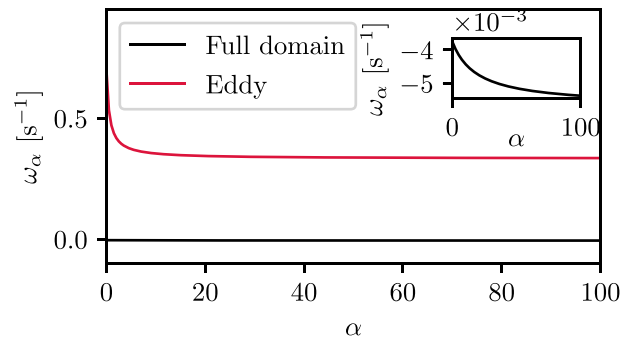


Fig. 7. The rigid-body angular velocity defined by (54) calculated for the AVISO dataset featured in Fig. 4. The black curve shows the angular velocity calculated over the full domain shown in Fig. 4. The red curve shows the result of the calculation restricted to the neighborhood of the mesoscale eddy shown in the insets of Fig. 4. (For interpretation of the references to color in this figure legend, the reader is referred to the web version of this article.)

[8] T. Kreilos, S. Zammert, B. Eckhardt, Comoving frames and symmetry-related motions in parallel shear flows, *J. Fluid Mech.* 751 (2014) 685–697.
 [9] H.J. Lugt, The dilemma of defining a vortex, in: U. Müller, K.G. Roesner, B. Schmidt (Eds.), *Recent Developments in Theoretical and Experimental Fluid Mechanics*, Springer-Verlag, 1979, pp. 309–321.
 [10] C. Truesdell, W. Noll, *The Non-Linear Field Theories of Mechanics*, Springer, 2004.
 [11] S.B. Pope, *Turbulent Flows*, Cambridge University Press, 2000.
 [12] C.G. Speziale, A review of material frame-indifference in mechanics, *Appl. Mech. Rev.* 51 (8) (1998) 489–504.
 [13] G.B. Arfken, H.J. Weber, *Mathematical Methods for Physicists*, Elsevier, Boston, 2005.
 [14] H. Lamb, *Hydrodynamics*, Dover, 1945.
 [15] P. Constantin, An Eulerian-Lagrangian approach to the Navier-Stokes equations, *Comm. Math. Phys.* 216 (3) (2001) 663–686.
 [16] R.G. Littlejohn, M. Reinsch, Gauge fields in the separation of rotations and antireal motions in the n-body problem, *Rev. Modern Phys.* 69 (1997) 213–276.
 [17] G. Batchelor, *An Introduction to Fluid Dynamics*, Cambridge University Press, 2000.
 [18] V. Kolář, Vortex identification: New requirements and limitations, *Int. J. Heat Fluid Flow* 28 (4) (2007) 638–652.
 [19] C. Liu, Y. Gao, S. Tian, X. Dong, Rortex—A new vortex vector definition and vorticity tensor and vector decompositions, *Phys. Fluids* 30 (3) (2018) 035103.
 [20] Y.-q Wang, Y.-s. Gao, J.-m. Liu, C. Liu, Explicit formula for the Liutex vector and physical meaning of vorticity based on the Liutex-Shear decomposition, *J. Hydrodyn.* 31 (3) (2019) 464–474.
 [21] B. Holmedal, Spin and vorticity with vanishing rigid-body rotation during shear in continuum mechanics, *J. Mech. Phys. Solids* 137 (2020) 103835.
 [22] P. Neff, J. Lankeit, A. Madeo, On Grioli’s minimum property and its relation to Cauchy’s polar decomposition, *Internat. J. Engrg. Sci.* 80 (2014) 209–217.
 [23] R. Bujack, M. Hlawitschka, K.I. Joy, Topology-inspired Galilean invariant vector field analysis, in: *2016 IEEE Pacific Visualization Symposium (PacificVis)*, IEEE, Taipei, Taiwan, 2016, pp. 72–79.
 [24] T. Günther, M. Gross, H. Theisel, Generic objective vortices for flow visualization, *ACM Trans. Graph.* 36 (4) (2017) 1–11.
 [25] B. Kim, T. Günther, Robust reference frame extraction from unsteady 2D vector fields with convolutional neural networks, *Comput. Graph. Forum* 38 (3) (2019) 285–295.
 [26] I.B. Rojo, T. Günther, Vector field topology of time-dependent flows in a steady reference frame, *IEEE Trans. Vis. Comput. Graphics* 26 (2020) 280–290.
 [27] T. Günther, H. Theisel, Hyper-objective vortices, *IEEE Trans. Vis. Comput. Graphics* 26 (3) (2020) 1532–1547.
 [28] G. Haller, Can vortex criteria be objectivized? *J. Fluid Mech.* 908 (2021) A25.
 [29] H. Theisel, M. Hadwiger, P. Rautek, T. Theußl, T. Günther, Vortex criteria can be objectivized by unsteadiness minimization, *Phys. Fluids* 33 (10) (2021) 107115.
 [30] M. Hadwiger, M. Mlejnek, T. Theußl, P. Rautek, Time-dependent flow seen through approximate observer killing fields, *IEEE Trans. Vis. Comput. Graphics* 25 (1) (2019) 1257–1266.

- [31] P. Rautek, M. Mlejnek, J. Beyer, J. Troidl, H. Pfister, T. Theußl, M. Hadwiger, Objective observer-relative flow visualization in curved spaces for unsteady 2D geophysical flows, *IEEE Trans. Vis. Comput. Graphics* 27 (2) (2021) 283–293.
- [32] X. Zhang, M. Hadwiger, T. Theußl, P. Rautek, Interactive exploration of physically-observable objective vortices in unsteady 2D flow, *IEEE Trans. Vis. Comput. Graphics* (2021) 1.
- [33] G. Astarita, Objective and generally applicable criteria for flow classification, *J. Non-Newton. Fluid Mech.* 6 (1) (1979) 69–76.
- [34] M. Tabor, I. Klapper, Stretching and alignment in chaotic and turbulent flows, *Chaos Solitons Fractals* 4 (6) (1994) 1031–1055.
- [35] G. Lapeyre, P. Klein, B.L. Hua, Does the tracer gradient vector align with the strain eigenvectors in 2D turbulence? *Phys. Fluids* 11 (12) (1999) 3729–3737.
- [36] C. Liu, Y.-s. Gao, X.-r. Dong, Y.-q. Wang, J.-m. Liu, Y.-n. Zhang, X.-s. Cai, N. Gui, Third generation of vortex identification methods: Omega and Liutex/Rortex based systems, *J. Hydrodyn.* 31 (2) (2019) 205–223.
- [37] J. Liu, Y. Gao, C. Liu, An objective version of the Rortex vector for vortex identification, *Phys. Fluids* 31 (6) (2019) 065112.
- [38] J.-m. Liu, Y.-s. Gao, Y.-q. Wang, C. Liu, Objective Omega vortex identification method, *J. Hydrodyn.* 31 (3) (2019) 455–463.
- [39] C. Liu, H. Xu, X. Cai, Y. Gao, *Liutex and Its Applications in Turbulence Research*, Academic Press, Cambridge, Massachusetts, 2020.
- [40] M. Serra, G. Haller, Objective Eulerian coherent structures, *Chaos* 26 (5) (2016) 053110.
- [41] H. Goldstein, C.P. Poole, J.L. Safko, *Classical Mechanics*, third ed., Addison Wesley, 2008.
- [42] A. Tachibana, T. Iwai, Complete molecular Hamiltonian based on the Born–Oppenheimer adiabatic approximation, *Phys. Rev. A* 33 (4) (1986) 2262–2269.
- [43] J.E. Marsden, *Lectures on Mechanics*, in: London Mathematical Society Lecture Note Series No. 174, Cambridge University Press, Cambridge, England, 1992.
- [44] C. Eckart, Some studies concerning rotating axes and polyatomic molecules, *Phys. Rev.* 47 (1935) 552–558.
- [45] T. Bergeron, Über die dreidimensional verknüpfende wetteranalyse I, *Geof. Publ.* 5 (6) (1928).
- [46] J. Pedlosky, *Geophysical Fluid Dynamics*, Springer New York, 1987.
- [47] G. Haller, Lagrangian coherent structures, *Annu. Rev. Fluid Mech.* 47 (2015) 137–162.
- [48] B. Epps, Review of vortex identification methods, in: 55th AIAA Aerospace Sciences Meeting, AIAA, 2017, pp. 1–22.
- [49] T. Günther, H. Theisel, The state of the art in vortex extraction, *Comput. Graph. Forum* 37 (6) (2018) 149–173.
- [50] A.M. Mancho, S. Wiggins, J. Curbelo, C. Mendoza, Lagrangian descriptors: A method for revealing phase space structures of general time dependent dynamical systems, *Commun. Nonlinear Sci. Numer. Simul.* 18 (2013) 3530–3557.
- [51] T. Pedergrana, D. Oettinger, G. P. Langlois, G. Haller, Explicit unsteady Navier–Stokes solutions and their analysis via local vortex criteria, *Phys. Fluids* 32 (4) (2020) 046603.
- [52] F. Lekien, G. Haller, Unsteady flow separation on slip boundaries, *Phys. Fluids* 20 (9) (2008) 097101.
- [53] J. Zhu, L.E. Holmedal, A numerical study of separation and stagnation points for steady and unsteady flow over an elliptic cylinder near a moving wall, *Phys. Fluids* 33 (8) (2021) 083617.
- [54] P.Y. Le Traon, F. Nadal, N. Ducet, An improved mapping method of multisatellite altimeter data, *J. Atmos. Ocean. Technol.* 15 (2) (1998) 522–534.
- [55] T. Tél, L. Kadi, I.M. Jánosi, M. Vincze, Experimental demonstration of the water-holding property of three-dimensional vortices, *Europhys. Lett. (EPL)* 123 (2018) 44001.
- [56] T. Dombre, U. Frisch, J.M. Greene, M. Hénon, A. Mehr, A.M. Soward, Chaotic streamlines in the ABC flows, *J. Fluid Mech.* 167 (1986) 353–391.